A steady MHD natural convection and heat transfer fluid flow through a vertical surface in the existence of hall current and radiation

Rajib Biswas[1,*], Munmun Mondal[1], Ariful Islam[2]

1. Mathematics Discipline, Science, Khulna University, Khulna-9208, Bangladesh

2. Department of Chemical Engineering, University of Newcastle
   NSW-2308, Australia

   rajibkumath11@gmail.com

ABSTRACT. *MHD heat disposal fluid flow within a vertical surface in the attendance of Hall current is smeared in this recent paper. The leading partial differential equations (PDEs) are motamorposhosed into dimensionless coupled of partial differential equations (PDEs) by the as usual mathematical procedure of transformation and the resultant equations are numerically evaluated by applying the explicit finite difference method (EFDM). The numerical outcome of velocity (primary and secondary) and temperature profiles are computed with the helps of COMPAQ VISUAL FORTRAN (CVF) 6.6a for the variations of various non-dimensional parameters such as magnetic parameter (M), Grashof number (Gr), Prandtl number (Pr), Hall parameter (m), permeability of porous medium (Kp) and radiation parameter (Ra) which values are chosen after stability convergence test (SCT). Furthermore, the effects of different system parameters on skin friction, Nusselt and Sherwood number are exhibited graphically. In addition, the Streamlines and isotherms have been investigated for different interesting parameters in this article. At the end the acquired results are plotted by using TECPLOT-9 (graphics software) and these are cultivated with graphically.*

RÉSUMÉ. *L'écoulement de fluide d'évacuation thermique MHD sur une surface verticale en présence du courant de Hall est étalé dans le présent article. Les équations aux dérivées partielles (EDP) dominantes sont motamorposées en couplage sans dimension d'EDP par la procédure mathématique habituelle de transformation et les équations résultantes sont évaluées numériquement en appliquant la méthode des différences explicites finies (EFDM). Les résultats numériques des profils de vitesse et de température sont calculés à l'aide de logiciel COMPAQ VISUAL FORTRAN (CVF) 6.6a pour les variations de divers paramètres non dimensionnels tels que le paramètre magnétique (M), le nombre de Grashof (Gr), le nombre de Prandtl (Pr), le paramètre de Hall (m), la perméabilité du milieu poreux (Kp) et le paramètre de rayonnement (Ra) après analyse de la convergence de la stabilité (SCA). En outre, les effets de différents paramètres du système sur le frottement superficiel, le nombre de Nusselt et de Sherwood sont présentés graphiquement. De plus, les lignes de courant et les lignes isothermes*

ont été étudiés pour différents paramètres intéressants dans cet article. A la fin, les résultats acquis sont tracés à l'aide de TECPLOT-9 (logiciel graphique) et sont cultivés avec des graphiques.

1. Introduction

The voltage difference through an electrical conductor and vertical to an electric current in the conductor where a magnetic field which is perpendicular to the current is called Hall effect. Now a days, the phenomenon of Hall current effect and heat transfer are applicable in science and technology. The Hall effects was first revealed experimentally by Edwin Hall in 1879. Also, during the recent years, MHD natural convection plays a vital role in geophysics, engineering and technological fields. In a rotating system, MHD free convection fluid flow of mass transfer past an oscillatory porous plate in the presence of Hall, ion-slip currents and heat source have been cultivated by Hossain *et al.* (2015). Unsteady MHD free convective flow through an accelerated plate with Hall effects was well-acquainted by Shankar et Yirga (2013). Also, the magnetohydrodynamic (MHD) Casson fluid flow over a stretching cylinder has been investigated by Biswas et Ahmmed (2018), Tamoor *et al.* (2017), Das *et al.* (2016), Attia (2005, 2006, 2007) and Pattnaik *et al.* (2016) have sacrifced the diffusion-thermo effect, MHD and Hall current effects. It is observed from their research activity that the velocity reduces with an increase in both suction and injection. Transient MHD free convection, mass transfer flow past an infinite perpendicular plate in a rotating system, with the consideration of Hall current has been studied by Ahmed et Kalita (2011). Mass transfer and Hall effects on oscillatory hydromantic through a perpendicular porous flat surface has been carried out by Biswal *et al.* (1994). Also, Kumar et Sahoo (2016) have argued the swirling flow.

Magnetohydrodynamics (MHD) is the schooling of a continuous, electrically conducting fluid under the impact of magnetic fields. MHD analysis deals with many ordinary phenomena and engineering problems. Now a days, there are many applications of MHD such as petro-chemical industry, heat exchanger design and geophysics, cooling of nuclear reactors as well as magnetohydrodynamics power generation system. Also, MHD free convection flows are applicable in fibre and granular insulation, geothermal systems etc. The cosmos is filled with extensively spaced charged particles and permeated by magnetic fields. Further, MHD is useful in astrophysics. The unsteady couette flow in the considering of Ion-slip has been researched by Attia. Also, Islam *et al.* have searched the incompressible fluid flow past a cellular plate in the presence of induced magnetic field. Casson fluid flow using the homology analysis method (HAM) has been abandonted by Animasaun *et al.* Casson fluid flow between a parallel plates was elaborated by Ahmed *et al.* (2017). The unsteady hydromagnetic flow with diffusion- thermo effect, Hall current was found by Pattnaik *et al.* (2013) and heat and mass transfer was discussed by Rajput et

Chad (1017). MHD flow of nanofluids past a stretching sheet was captialized by Shankar *et al.* (2016), Animasaun *et al.* (2016), Ali (2014), Venkateswarlu *et al.* (2017), Sharma *et al.* (2018) and bifurcation and stability of forced convection was analysed by Wang et Yang (2004).

Radiation is the heat from the sun, the heat is radiated through space to our planet without the aid of fluids or solids. Also, the electromagnetic radiation is through a given frequency and which is proportional to the amount of absorption heat. Furthermore, boundary layer phenomena occurs when the influence of a physical quantity is restricted to small regions or when the non-dimensional diffusion parameters such as the Reynolds number is very large. Further, the boundary layers are proportional to the square root of the associated diffusion number. Like MHD behaviour, chemical reactions also an unabated term in fluid mechanics in recent times due to its technological and engineering interest. Burning fuels, smelting iron, brewing beer and making wine and cheese are very common precedent for long time of incorporating chemical reactions. Physical changes include changes of state, such as ice melting to water and water evaporating to vapour. MHD casson fluid flow through an oscillating perpendicular plate with radiation and chemical reaction effects has beeen practised by Kataria et Patel (2016), Islam *et al.* (2011), Rohsenow *et al.* (1998), Makinde *et al.* (2017, 2018). Also, the MHD casson fluid flow has been introduced by Biswas *et al.* (2017, 2018). Effects of Hall current and chemical reaction on MHD unsteady heat and mass transfer of casson nanofluid flow through a vertical plate was performed by Biswas *et al.* (2018). Unsteady magnetohydrodynamic free convection flow of nanofluid through an exponentially accelerated inclined plate embedded in a porous medium with variable thermal conductivity in the presence of radiation was recently contibuted by Ahmmed *et al.* (2018). These types of work are recently published by Balocco and Petrone (2018); Garg *et al.* (2017); Sun *et al.* (2017) and Chaware *et al.* (2017).

However, the motivation of this recent reasearch is to study the effects of Hall current of heat transfer fluid flow. Basically, here we have obtained the steady state solution of our proiblem. A mathematical solution of the flow governing model equations which includes the transient momentum and energy equations. These equations are solved numerically by using explecit finite difference method (EFD M) after non-dimensional. The closed numerical solutions has been evaluated for the velocity and temperature profile after stability and convergence analysis (SCA) by using FORTRAN language. The effect of different parameters on velocity and temperature distributions are calculated and presented graphically with overall discussions.

2. Mathematical formulation

Consider an electrically conducting unsteady MHD incompressible fluid as well as viscous fluid flow through a perpendicular cellular surface in the force of permeability of porous medium and Hall current. The anatomical synopsis of the model is demonstrated in the Figure 1. In this research work, *x*-axis is taken into the perpendicular surface and the *y*-axis is normal to the surface. It is assume that an

identical magnetic field strength B_0 is acted transversely to the way of fluid flow and which is ignored due to the small Reynolds number. So that the magnetic field is $B=(0, B_0, 0)$. The equation of preservation of charge is considered as $\nabla.J=0$ where J_y=constant. Along the y-axis, J does not have any change in y-axis i.e. J_y=0. According to Cowling,

$$J + \frac{W_e \tau_e}{B_0}(J \times B) = \sigma(q \times B) + \frac{1}{e\eta_e}\nabla P_e \tag{1}$$

where q is velocity vector, B is magnetic field vector, J is current density vector, e is electric charge, σ is electric conductivity, ω_e is cyclotron frequency, τ_e is electron collision time, B_0 is uniform magnetic field of strength, P_e is electron frequency and η_e is number of density of electrons.
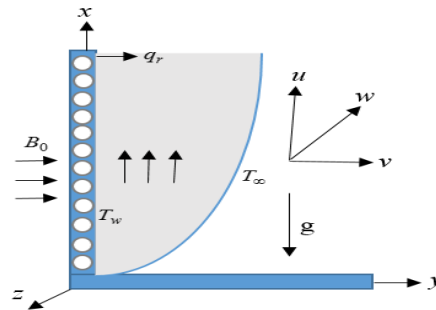
Figure 1. Physical configurations and coordinate system

Also, we supposed that the plate temperature is T_w. But at time $t>0$, the temperature is out side the layer is T_∞ with time τ. According to Das *et al.* (2016), the primary and secondary velocity can found by the following equations:

$$\frac{\partial u}{\partial t} + u\frac{\partial u}{\partial x} + v\frac{\partial u}{\partial y} = v\frac{\partial^2 u}{\partial y^2} + g\beta_T(T - T_\infty) - \frac{v}{k^*}u + \frac{B_0}{\rho}J_z \tag{2}$$

$$\frac{\partial w}{\partial t} + u\frac{\partial w}{\partial x} + v\frac{\partial w}{\partial y} = v\frac{\partial^2 w}{\partial y^2} - \frac{v}{k^*}w - \frac{B_0}{\rho}J_x \tag{3}$$

Under these assumptions the dimensional primary velocity, secondary velocity and temperature equations of the present problem can be expressed as:

$$\frac{\partial u}{\partial x} + \frac{\partial v}{\partial y} = 0 \tag{4}$$

$$\frac{\partial u}{\partial t} + u\frac{\partial u}{\partial x} + v\frac{\partial u}{\partial y} = v\frac{\partial^2 u}{\partial y^2} + g\beta_T(T - T_\infty) - \frac{v}{k^*}u - \frac{\sigma B_0^2(u+mw)}{\rho(1+m^2)} \tag{5}$$

$$\frac{\partial w}{\partial t} + u\frac{\partial w}{\partial x} + v\frac{\partial w}{\partial y} = v\frac{\partial^2 w}{\partial y^2} - \frac{v}{k^*}w + \frac{\sigma B_0^2(mu-w)}{\rho(1+m^2)} \tag{6}$$

$$\frac{\partial T}{\partial t} + u\frac{\partial T}{\partial x} + v\frac{\partial T}{\partial y} = \frac{k}{\rho C_p}\frac{\partial^2 T}{\partial y^2} - \frac{1}{\rho C_p}\frac{\partial q_r}{\partial y} + \frac{Q}{\rho C_p}(T - T_\infty) \tag{7}$$

$$\left.\begin{array}{l} t = 0, u = 0, v = 0, w = 0, T = T_w \text{ at } y = 0 \\ t > 0, u = 0, v = 0, w = 0, T \to T_\infty \text{ as } y \to \infty \end{array}\right\} \tag{8}$$

where, k^* is Darcy permeability, C_p is the specific heat at constant pressure, k is the thermal conductivity, ρ is the fluid density, g is the gravitational acceleration, β_T is the thermal expansion coefficient, and q_r is the radiated heat flux. By the Rohsenow *et al.* (1998) approximation radiation effect can be defined as

$$q_r = -\frac{4\sigma'}{3k'}\frac{\partial T^4}{\partial y} \tag{9}$$

where σ' is the Slefan-Boltzmann constant and k' is the mean absorption constant respectively. It is assumed that temperature differences are sufficiently small and T^4 may be obtained as:

$$T^4 \approx T_\infty^4 + 4T_\infty^3 T - 4T_\infty^3 T_\infty \approx 4T_\infty^3 T - 3T_\infty^4$$

$$\therefore \frac{\partial q_r}{\partial y} = -\frac{16\sigma' T_\infty^3}{3k'}\frac{\partial^2 T}{\partial y^2} \tag{10}$$

Due to the solutions of EFDM, the obtained equations can be evslusted dimensionless and choose the variables as:

$$U = \frac{u}{U_0}; V = \frac{v}{U_0}; W = \frac{w}{U_0}; Y = \frac{yU_0}{v}; X = \frac{xU_0}{v}; \tau = \frac{tU_0^2}{v}$$

$$T = T_\infty + \bar{T}(T_w - T_\infty) \tag{11}$$

By substituting the above values and its derivatives into the equations (4) to (8) we obtained,

$$\frac{\partial U}{\partial X} + \frac{\partial V}{\partial Y} = 0 \tag{12}$$

$$\frac{\partial U}{\partial \tau} + U\frac{\partial U}{\partial X} + V\frac{\partial U}{\partial Y} = \frac{\partial^2 U}{\partial Y^2} + G_r\bar{T} - M\frac{U+mW}{1+m^2} - K_p U \tag{13}$$

$$\frac{\partial W}{\partial \tau} + U\frac{\partial W}{\partial X} + V\frac{\partial W}{\partial Y} = \frac{\partial^2 W}{\partial Y^2} - M\frac{W-mU}{1+m^2} - K_p W \tag{14}$$

$$\frac{\partial \bar{T}}{\partial \tau} + U\frac{\partial \bar{T}}{\partial X} + V\frac{\partial \bar{T}}{\partial Y} = \frac{1}{P_r}\frac{\partial^2 \bar{T}}{\partial Y^2} + R_a\frac{\partial^2 \bar{T}}{\partial Y^2} + \alpha\bar{T} \tag{15}$$

Also, we get the associate boundary conditions,

$$\left.\begin{array}{l} \tau = 0, U = 0, V = 0, W = 0, \bar{T} = 1 \text{ at } Y = 0 \\ \tau > 0, U = 0, W = 0, \bar{T} \to 0 \text{ as } Y \to \infty \end{array}\right\} \tag{16}$$

where, Prandlt number: $P_r = \frac{\upsilon\rho C_p}{k}$; Grashof number: $G_r = \frac{\upsilon g\beta_T(T_W - T_\infty)}{U_0^3}$; Heat source

parameter: $\alpha = \frac{Q\upsilon}{\rho C_p U_0^2}$; magnetic parameter: $M = \frac{\sigma B_0^2\upsilon}{\rho U_0^2}$; Radiation parameter: $R_a = \frac{4\sigma'T_\infty^3}{k'k}$; Hall parameter: $m = \omega_e\tau_e$.

The skin friction, Nuselt and Sherwood number are obtained as:

$$C_f = -\frac{1}{2\sqrt{2}}(G_r)^{-\frac{3}{4}}\left(\frac{\partial U}{\partial Y}\right)_{Y=0}, N_u = \frac{1}{\sqrt{2}}(G_r)^{-\frac{3}{4}}\left(\frac{\partial \bar{T}}{\partial Y}\right)_{Y=0}, S_h = \frac{1}{\sqrt{2}}(G_r)^{-\frac{3}{4}}\left(\frac{\partial \bar{C}}{\partial Y}\right)_{Y=0}.$$

Stream function is denoted as $\psi(X,Y)$ and its component are given below as:

$$U = \frac{\partial\psi}{\partial Y}, V = -\frac{\partial\psi}{\partial X}.$$

3. Calculation technique

The obtained non-dimensional couple PDEs (12) to (17), have been solved by applying the EFDM. Here, it is considered that plate height is $X_{max}(=125)$ and $Y_{max}(=150)$. Also, we have assumed the grid spacing m=150 and n=300. All these observation are shown in the Figure 1(a). Further, $\Delta X=0.83$ $(0{\le}X{\le}125)$ and $\Delta Y=0.50$ $(0{\le}Y{\le}150)$ are taken the mesh sizes along X and Y axes with time-step, $\Delta\tau=0.0005$ and U', W' and $\bar{T}'$ denote the values of U, W and $\bar{T}$ at the end of a time-step.
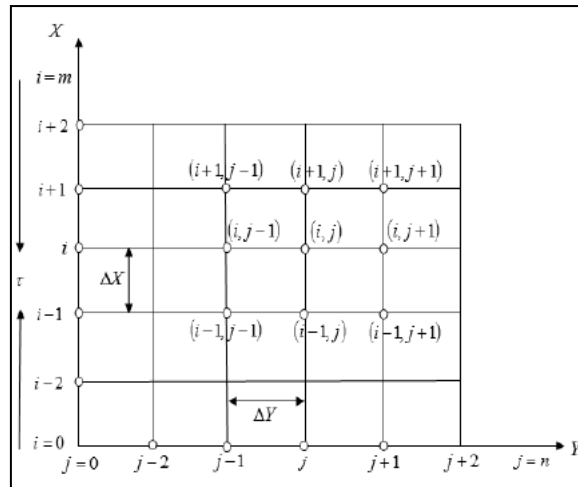
Figure 1(a). The finite difference space grid

Therefore by using EFDM we get the equations as:

$$\frac{U_{i,j}-U_{i-1,j}}{\Delta X} + \frac{V_{i,j}-V_{i,j-1}}{\Delta Y} = 0 \tag{17}$$

$$\frac{U'_{i,j}-U_{i,j}}{\Delta\tau} + U_{i,j}\left(\frac{U_{i,j}-U_{i-1,j}}{\Delta X}\right) + V_{i,j}\left(\frac{U_{i,j+1}-U_{i,j}}{\Delta Y}\right) = \left(\frac{U_{i,j+1}-2U_{i,j}+U_{i,j-1}}{(\Delta Y)^2}\right) + G_r\bar{T}_{i,j} -$$
$$M\left(\frac{U_{i,j}+mW_{i,j}}{1+m^2}\right) - k_p U_{i,j} \tag{18}$$

$$\frac{W'_{i,j}-W_{i,j}}{\Delta\tau} + U_{i,j}\left(\frac{W_{i,j}-W_{i-1,j}}{\Delta X}\right) + V_{i,j}\left(\frac{W_{i,j+1}-W_{i,j}}{\Delta Y}\right) = \left(\frac{W_{i,j+1}-2W_{i,j}+W_{i,j-1}}{(\Delta Y)^2}\right) -$$
$$M\left(\frac{W_{i,j}-mU_{i,j}}{1+m^2}\right) - k_p W_{i,j} \tag{19}$$

$$\frac{\bar{T}'_{i,j}-\bar{T}_{i,j}}{\Delta\tau} + U_{i,j}\frac{\bar{T}_{i,j}-\bar{T}_{i-1,j}}{\Delta X} + V_{i,j}\frac{\bar{T}_{i,j+1}-\bar{T}_{i,j}}{\Delta Y} = \frac{1}{P_r}\frac{\bar{T}_{i,j+1}-2\bar{T}_{i,j}+\bar{T}_{i,j-1}}{(\Delta Y)^2} + R_a\frac{\bar{T}_{i,j+1}-2\bar{T}_{i,j}+\bar{T}_{i,j-1}}{(\Delta Y)^2} +$$
$$\alpha\bar{T}_{i,j} \tag{20}$$

In this case, boundary conditions in explicite finite different method are obtained as:

$$\left.\begin{array}{l} U^n_{i,0} = 0, V^n_{i,0} = 0, W^n_{i,0} = 0, \bar{T}^n_{i,0} = 1 \\ U^n_{i,L} = 0, W^n_{i,L} = 0, \bar{T}^n_{i,L} \to 0 \text{ where } L \to \infty \end{array}\right\} \tag{21}$$

Here i and j designate to the mesh points.

4. Stability and convergence analysis

The stability conditions for the present problem are,

$$\frac{2\Delta\tau}{(\Delta Y)^2} + \frac{M\Delta\tau}{1+m^2} + U\frac{\Delta\tau}{\Delta X} + |-V|\frac{\Delta\tau}{\Delta Y} + \frac{K_p\Delta\tau}{2} \le 1 \tag{22}$$

$$\left(R_a + \frac{1}{P_r}\right)\frac{2\Delta\tau}{(\Delta Y)^2} + U\frac{\Delta\tau}{\Delta X} + |-V|\frac{\Delta\tau}{\Delta Y} - \frac{Q\Delta\tau}{2} \le 1 \tag{23}$$

By using initial conditions, $U=W=0$ at $\tau=0$, we get the convergence criteria of the equations (22) to (23) are $P_r \geq 0.34$ and $R_a \geq 0.30$.

5. Results and discussion

An explicit finite difference method (EFDM) has been used to obtain the results of the present problem and the numerical values are evaluated by the variations of various parameters. The primary velocity, secondary velocity, temperature, skin friction coefficient, Nusselt number, Sherwood number, streamlines and isotherms are obtained of the present model for the values of magnetic parameter (M), Hall parameter (m), permeability of porous medium (K_p), Prandtl number (P_r), Grashof number (G_r), heat source parameter (α) and radiation parameter (R_a). Here we have chosen the overall common values as: $M=3.00$, $P_r=0.71$(air), $R_a=0.50$, $m=0.20$, $\alpha=1.0$, $G_r=10$ and $K_p=1.0$. Also, we have considered the dimensionless time $\tau=10, 20, 30, 40, 50, 60, 70, 80$. The result changes for $\tau=10$-40 but when arising time more than it then

become steady-state. The values U versus Y, W versus Y and $\bar{T}$ versus Y are evaluated in the respective figures.

Figures. 2 to 5 are drawn with the variations of G_r (10.00, 15.00, 20.00) for dimensionless time τ=10, 20, 50, 80 respectively. Here, Pr=0.71, M=3.00, m=0.20, R_a=0.50, K_p=1.0 and α=1.00 are constant. It is found that U improve with the enhancement of G_r. But the profiles coincide once with the increase of Gr for τ=40 to 80. Physically, the G_r which produced a buoyancy force in the boundary layer. Due to this force which increse the fluid velocity. Here the steady-state solution continued for τ=50 to 80. Also, it is shown that temperature profiles are same with the improvement of G_r. But there is no impact over the temperature profiles. Therefore, the solutions occurs steady-state for all time intervals.
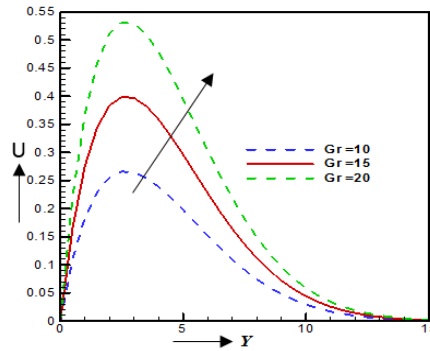
Figure 2. Effects of U for the variation of G_r against Y where M=3.00, P_r=0.71, R_a=0.50, k_p=1.0, m=0.20, α=1.00, and τ=10
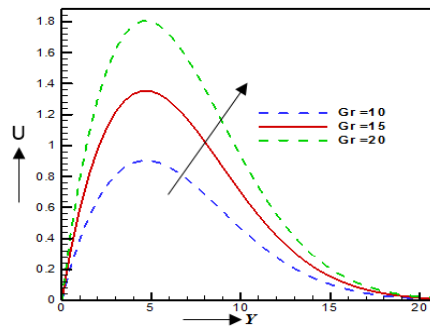
Figure 3. Impact of U for the variation of G_r against Y where M=3.00, P_r=0.71, R_a=0.50, k_p=1.0, m=0.20, α=1.00, and τ=20
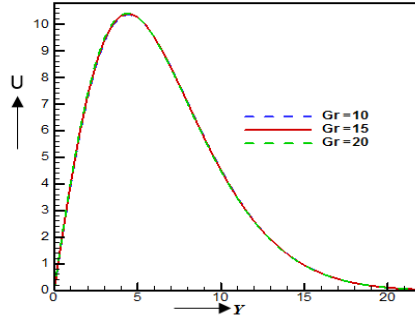
Figure 4. Influence of U for the variation of G_r against Y where M=3.00, P_r=0.71, R_a=0.50, k_p=1.0, m=0.20, α=1.00, and τ=50
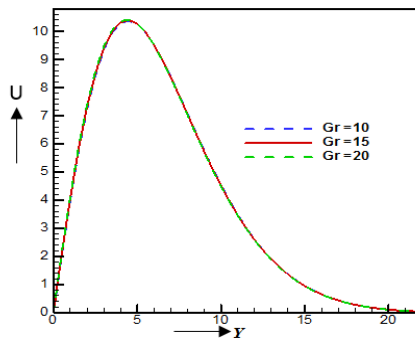
Figure 5. Variations of U for the variation of G_r against Y where M=3.00, P_r=0.71, R_a=0.50, k_p=1.0, m=0.20, α=1.00, and τ=80
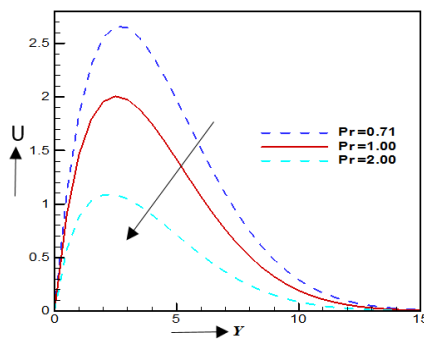
Figure 6. Despription of U for the variation of P_r against Y where G_r =10.00, M=3.00, R_a=0.50, k_p=1.0, m=0.20, α=1.00, and τ=10
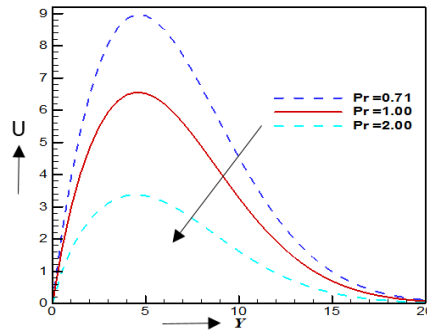
Figure 7. Representation of U for the variation of P_r against Y where G_r =10.00, M=3.00, R_a=0.50, K_p=1.0, m=0.20, α=1.00, and τ=20
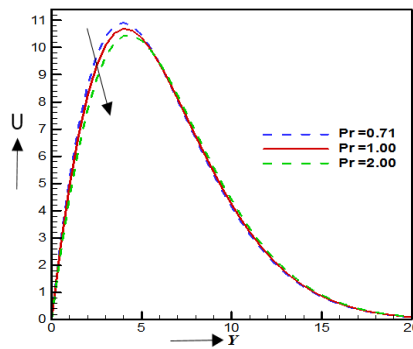
Figure 8. Elucidation of U for the variation of P_r against Y where G_r =10.00, M=3.00, R_a=0.50, k_p=1.0, m=0.20, α=1.00, and τ=50
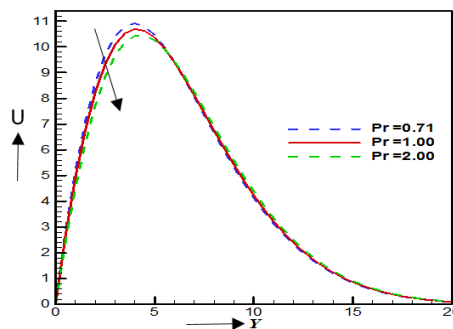
Figure 9. Explication of U for the variation of P_r against Y where G_r =10.00, M=3.00, R_a=0.50, k_p=1.0, m=0.20, α=1.00, and τ=80
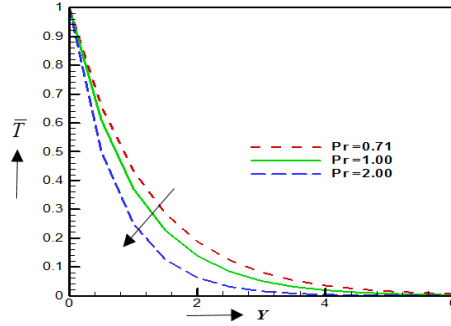
Figure 10. Depiction of $\bar{T}$ for the variation of P_r against Y where M=3.00, G_r =10.00, K_p=1.0, R_a=0.50, m=0.20, α=1.00, and τ=10
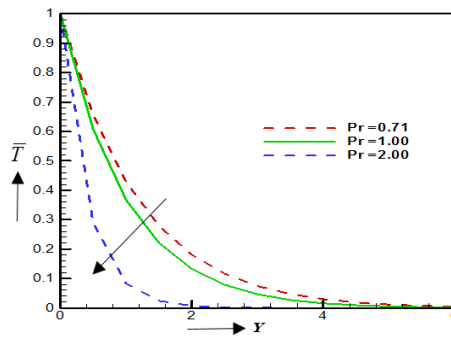
Figure 11. Vestige of $\bar{T}$ for the variation of P_r against Y where M=3.00, G_r =10, R_a=0.50, m=0.20, α=1.00, and τ=20
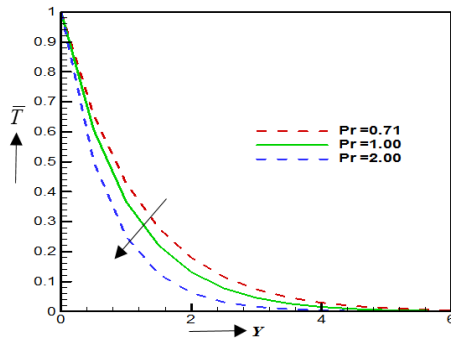
Figure 12. Painting of $\bar{T}$ for the variation of P_r against Y where M=3.00, G_r =10, R_a=0.50, m=0.20, α=1.00, and τ=70
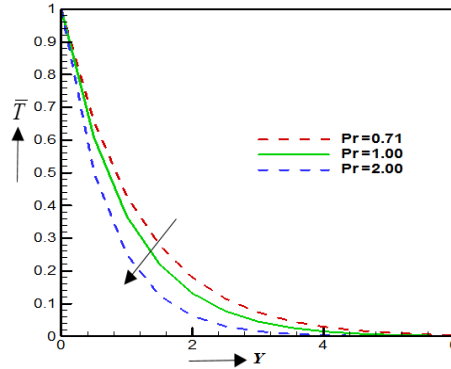
Figure 13. Variations of $\bar{T}$ for the different values of P_r where M=3.00, G_r =10, R_a=0.50, m=0.20, α=1.00, and τ=80

The influence of velocity and temperature profiles are displayed in the respective Figures 6-13 for various values of P_r= 0.71, 1.00, 2.00 for dimensionless time τ=10, 20, 70, 80 respectively. Here, G_r=10, M=3.00, m=0.20, R_a=0.50, K_p=1.0 and α=1.00 are constant. In Figures 6 to 9, it is observed that U is down with the headway of P_r. But the profiles coincide once and then increase with the rise of P_r for τ=50 to 80. Here, the steady-state solution continued for τ=50 to 80. Also, we found that temperature distributions decline 23.25%, and 0.09% at Y=0.35452 for P_r=0.71 to P_r=1.00, P_r=1.00 to P_r=2.00 which are shown in Figure 6, decreases at Y=0.36452 for P_r=0.71 to P_r=1.00, P_r=1.00 to P_r=2.00 which are found in Figure 7 and reduced 0.46% and 0.29% at Y=0.45672 for P_r=0.71 to P_r=1.00, P_r=1.00 to P_r=2.00 which are shown in Figures 10 to 13 respectively, but Figure 12 is coincide with 13. Naturally, this is due to the fluid with high P_r have high viscosity, which down the thermal boundary layer thickness i.e. for decays thermal boundary layer, heat transfer is reduced. Therefore, the steady condition occurs for all time intervals.
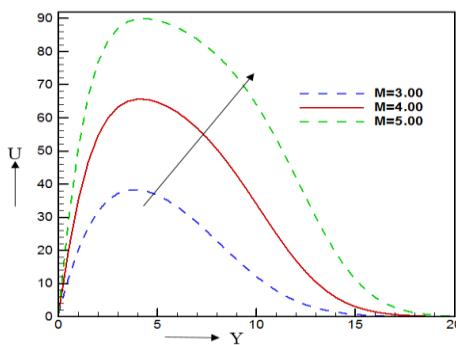

Figure 14. Graphs of U for the variation of M against Y where P_r =0.71, G_r =10, R_a=0.50, m=0.20, α=1.00, and τ=10
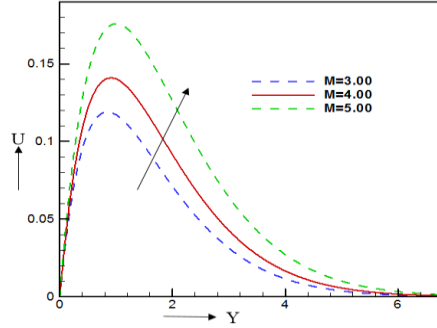
Figure 15. Illustration of U for the variation of M against Y where P_r =0.71, G_r =10, R_a=0.50, m=0.20, α=1.00, and τ=20
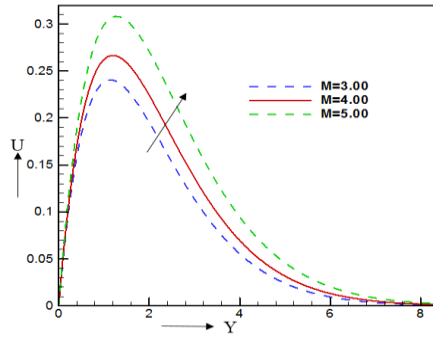

Figure 16. Illustration of U for the variation of M against Y where P_r =0.71, G_r =10, R_a=0.50, m=0.20, α=1.00, and τ=70
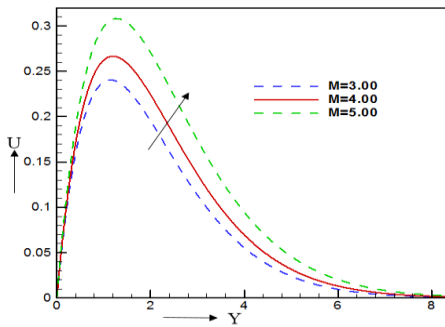

Figure 17. Velocity U for the variation of M against Y where P_r =0.71, G_r =10, R_a=0.50, m=0.20, α=1.00, and τ=80

The primary velocity distribusion are shown in the Figures 14 to 17 respectively with the variation of $G_r=10$, $P_r=0.71$, $m=0.20$, $R_a=0.50$, $K_p=1.0$ and $\alpha=1.00$ for dimensionless time $\tau=20$, 30, 70, 80 respectively. It is audited that from Figure 14 primary velocity cluim up 9.75% and 8.75% for $M=3.00$ to $M=4.00$, and $M=4.00$, to $M=5.00$. Similarly, from Figures 15 to 17 velocity profiles are progressed with the development of magnetic parameter (M). But the profiles approximately coincide once and improvement with the enhancement of M for $\tau=(70\text{-}80)$. Here the solutions are approximately steady-state for $\tau=40$ to 80. Here the steady-state solution occurs for all time intervals.

Figures 18 to 21 represents the graphs for various values of m= 0.50, 0.60, 0.70 for dimensionless time $\tau=10$, 20, 70, 80 respectively. Here, $M=0.50$, $P_r=0.71$, $m=0.20$, $R_a=0.50$ $K_p=1.0$ and $\alpha=1.00$ are constant. From Figures 18 to 21, it is preserved that U is reducing with the reduce of m. Generally, Hall current produced a resistive force. This resistive force decrease the velocity. But the profiles approximately coincide once and then completion with the rise of Hall parameter (m) for $\tau=40$ to 80. Here the solutions are approximately steady-state for $\tau=40$ to 80.
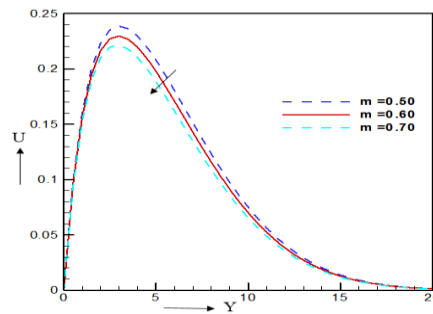

Figure 18. Graphical representation of U where M=3.00, P_r =0.71, G_r =10, R_a=0.50, α=1.00, and τ=10
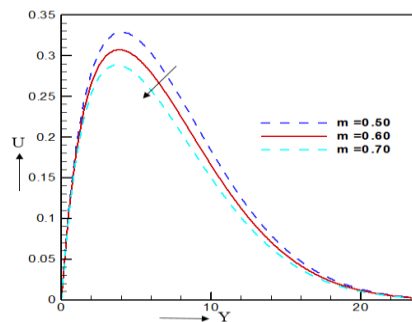

Figure 19. Graphs of U for the variation of m against Y where M=3.00, P_r =0.71, G_r =10, R_a=0.50, α=1.00, and τ=20
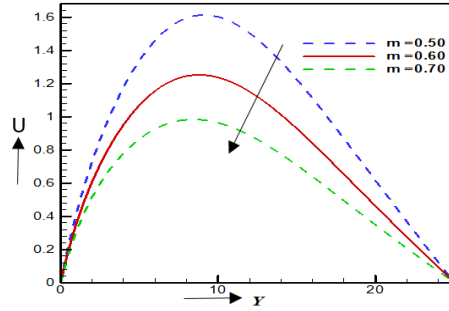
Figure 20. Velocity of U for the variation of m against Y where M=3.00, P_r =0.71, G_r =10, R_a=0.50, α=1.00, and τ=40
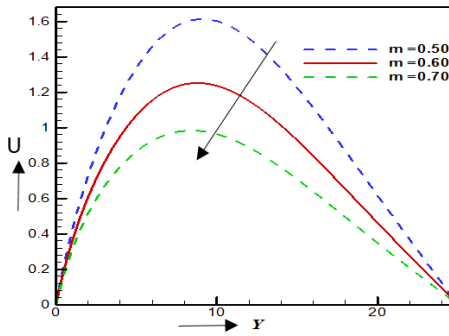

Figure 21. Illustration of U for the variation of m against Y where M=3.00, P_r =0.71, G_r =10, R_a=0.50, α=1.00, and τ=80
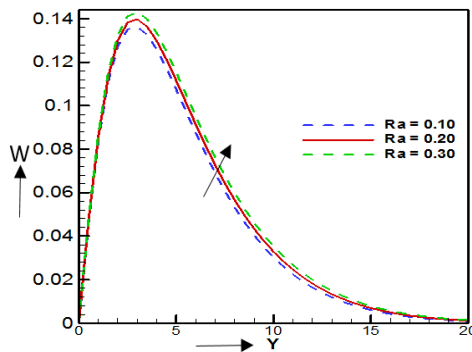

Figure 22. Illustration of W for the variation of R_a against Y where m=0.20, M=3.00, P_r =0.71, G_r =10, k_p=0.50, α=1.00, and τ=10
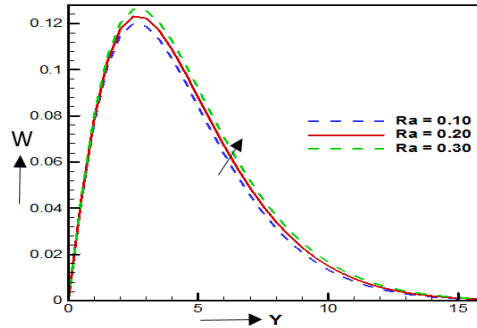
Figure 23. Effects of W for the variation of R_a against Y where m=0.20, M=3.00, P_r =0.71, G_r =10, k_p=0.50, α=1.00, and τ=20
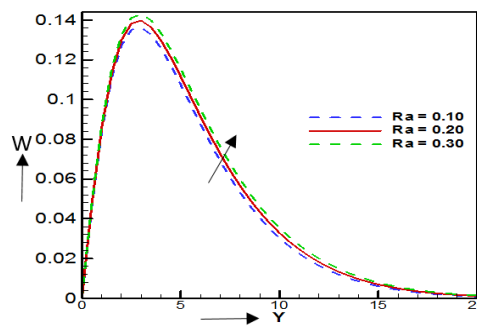
*Figure 24. Illustration of W for the variation of R_a against Y where m=0.20, M=3.00, P_r =0.71, G_r =10, k_p=0.50, α=1.00, and τ=60*
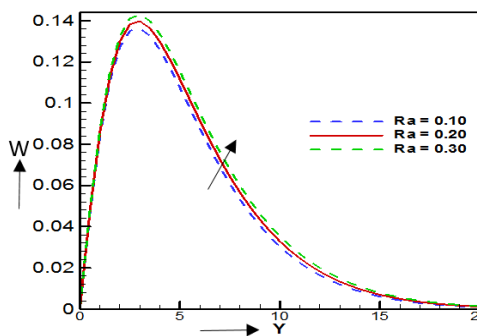
*Figure 25. Presentation of W for the variation of R_a where m=0.20, M=3.00, P_r =0.71, G_r =10, k_p=0.50, α=1.00, and τ=80*
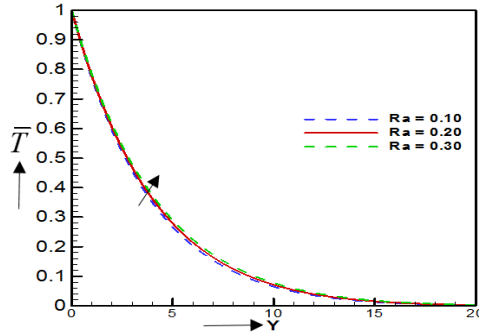
Figure 26. Impact of $\bar{T}$ for the variation of R_a against Y where m=0.20, M=3.00, P_r =0.71, G_r =10, k_p=0.50, α=1.00, and τ=10
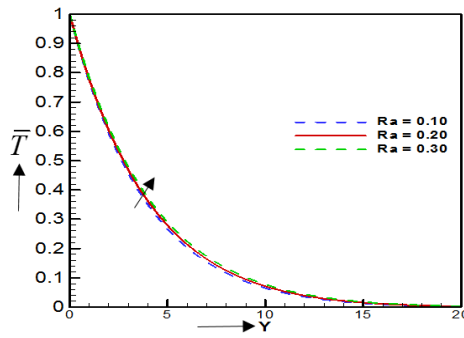
Figure 27. Temperature$\bar{T}$ for the variation of R_a where m=0.20, M=3.00, P_r =0.71, G_r =10, k_p=0.50, α=1.00, and τ=20
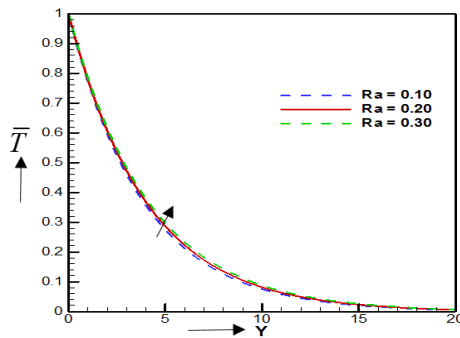
Figure 28. Influence of $\bar{T}$ for the variation of R_a where m=0.20, M=3.00, P_r =0.71, G_r =10, k_p=0.50, α=1.00, and τ=60
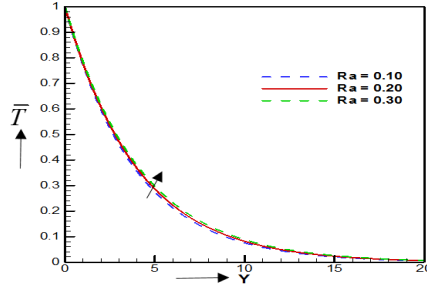
Figure 29. Illustration of $\bar{T}$ for the variation of R_a against Y where m=0.20, M=3.00, P_r =0.71, G_r =10, k_p=0.50, α=1.00, and τ=80

Secondary velocity profiles are exhibited in Figures 22 to 25 respectively for various values of R_a. There is an increment in the secondary velocity due to the improvement of R_a. From Figure 22, it is noticed that secondary velocity fulfilment 8.67% and 11.0% respectively as radiation parameter R_a changes from 0.10 to 0.20 and 0.20 to 0.30 at Y= 0.5560. But the profiles approximately coincide once and then compensation with the rise of R_a for τ=60 to 80. Also, temperature profiles are increament due to the raise of R_a which are exhibitated in the Figures 26 to 29. This enhancement is happened due to the raise of R_a, because which devoloped the thermal boundary layer.

For various values of K_p on secondary velocity and temperature are delimitated in Figure 30 to 33 respectively. From Figures 30, secondary velocity decreasing 14.41% and 27.26% as K_p changes from 0.50 to 1.50 and 1.50 to 2.50 respectively which occurs at time τ=10 with the increasing of K_p at Y=0.57750. The K_p which increases the resistive force. Due to this resistive force, primary and secondary velocity profiles are decreasing with the increasing of K_p. But the profiles approximately coincide once and then increase with the increase of K_p for τ=40 to 80. Therefore the solutions are approximately steady-state forτ=40 to 80. Also, temperature profiles are enhancement with the rise of K_p.
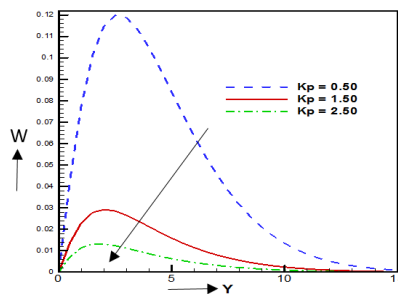
Figure 30. Representation of W for K_p against Y where m=0.20, M=3.00, R_a=0.5, P_r =0.71, G_r =10, k_p=0.50, α=1.00, and τ=10
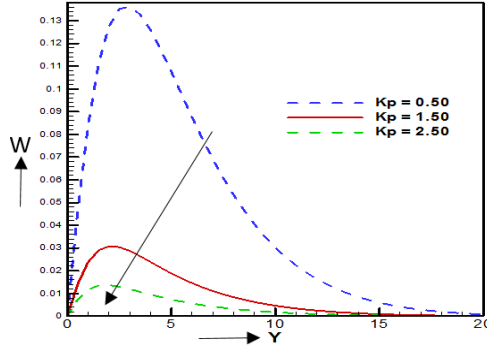
Figure 31. W for the variation of K_p against Y where m=0.20, M=3.00, R_a=0.5, P_r =0.71, G_r =10, k_p=0.50, α=1.00, and τ=20
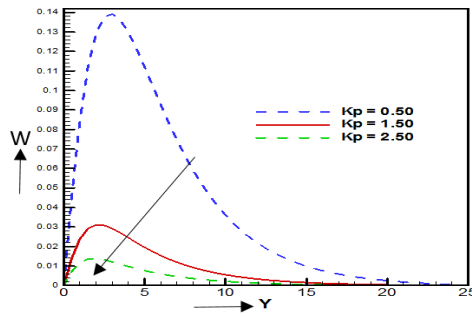
Figure 32. W for the variation of K_p against Y where m=0.20, M=3.00, R_a=0.5, P_r =0.71, G_r =10, k_p=0.50, α=1.00, and τ=40
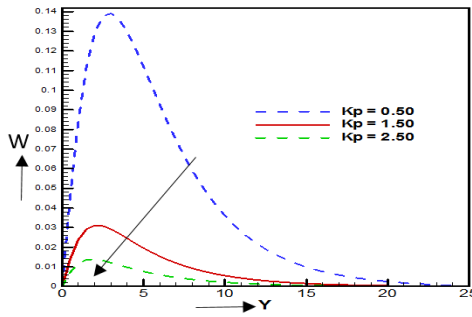
Figure 33. Secondary velocity W for K_p where m=0.20, M=3.00, R_a=0.5, P_r =0.71, G_r =10, k_p=0.50, α=1.00, and τ=80
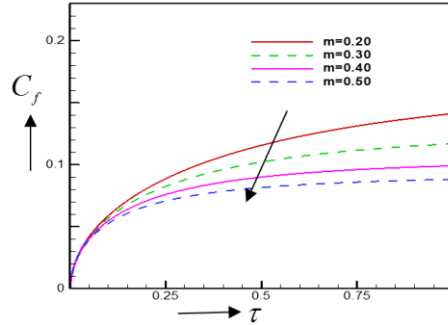
Figure 34. Skin friction for the variation of m against Y where M=3.00, P_r=0.71, R_a=0.50, α=1.00 and K_p=0.50
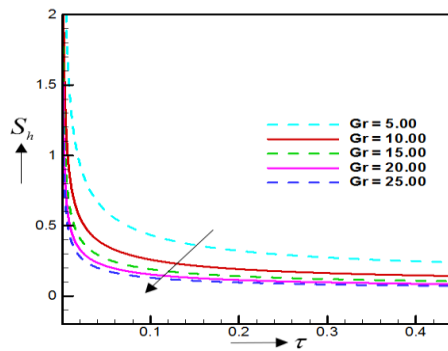
Figure 35. Sherwood number for the variation of G_r against Y where M=3.00, P_r=0.71, R_a=0.50, α=1.00 and K_p=0.50
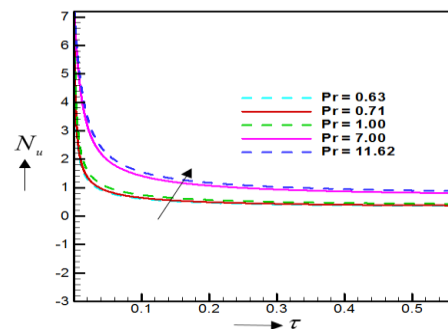
Figure 36. Nusselt number for the variation of P_r against Y where M=3.00, R_a=0.50, R_a=0.50, α=1.00 and K_p=1.0
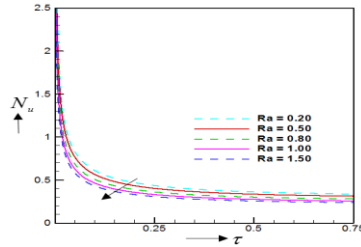
*Figure 37. Illustration Nusselt number for the variation of R_a against Y where M=3.00, P_r=0.71, α=1.00 and K_p=1.0*

The Figures 34 to 37 represents the effects of m, G_r, P_r and R_a on C_f, N_u and S_h. It is found that the C_f is down with the multiplication of m which is permit in the Figure 34. Physically, skin friction which is developed the rate of velocity of the fluid flow but here it is opposite. Also it is shown that form Figure 35, also S_h down with the growing of G_r this is way because by the downfall of convective mass transfer. On the other hand the Nusselt number is an improvement functions of P_r but abating the function of R_a. Generally, convective heat transfer rise with the augmentation of N_u.

The dimensionless equations are solved numerically by the doing of dimensoionless. Therefore, X and Y axis are dimensionless which presents the mash point i.e. numerical point of view. The difference of boundary layer for different parameters can be defined as stream and isotherms. The legend values (flood view) represents the stream and isotherms. Furthermore, streamlines profiles can be used to improve the visualization of fluid fields where the temperature remains constant (ΔT = 0). An isotherm at 0^0C is called the freezing level. The influence of M on streamlines and isotherms are represented in Figure 38 and Figure 39. Also, the streamlines and isotherms are aggrandizement due to the development of M in the Figure 38. Further, Figure 39 displays the thermal direction of fluid (thermal boundary layer thickness) with the benefit of two various magnetic parameter (M). The contours levels are also provided in the legend.
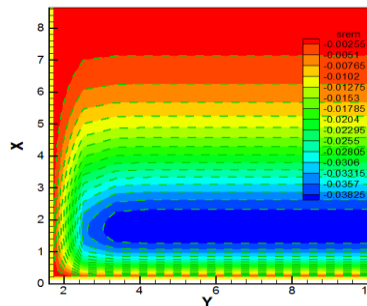
Figure 38. Streamlines for M=3.00, and M=4.00, (green dashed line) with flood view
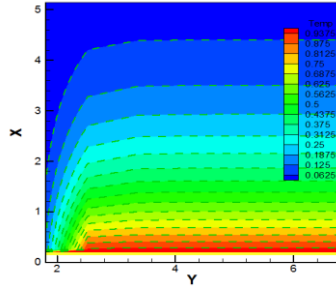
Figure 39. Effects of Isotherms for M=3.00, and M=4.00, (green dashed line) with flood view

Table 3. Represents the previous results by Kataria et Patel (2018)

Previous results by Kataria et Patel (2018).						
Increased parameters	U	T	C	Skin fri.	Nusl. Num.	Sher. Num.
G_r						
S	In c	In c				
S_r	In c					
M	Dec					
γ	Dec		Dec			In c
E_c						
P_r					In c	

Table 4. Represents the present results

Our present results						
Increased parameters	U	T	C	Skin fri.	Nusl. Num.	Sher. Num.
G_r	Inc					
S	In c	In c				
S_r	In c					
M	Dec					
γ	Dec		Dec			In c
E_c	Inc					
P_r		Dec			In c	

6. Conclusions

The following conclusions have been drawn by the above discussions:

(1) From the investigation we got that for the case of primary velocity profiles develop with the assemblage of Gr. But there is no effect on temperature profiles with the forward movement of Gr.

(2) It is pridicted that velocity profiles fall with the progession of Pr. Also, temperature profiles reduces with the advancement of Pr.

(3) It is found that, U put on with the promotion of M. On the other hand, there is no effect on temperature profiles.

(4) With the advancement of m, the velocity profiles minimizes. But there is no effect on temperature profiles with the dispersal of m.

(5) Nusselt are also flow on by Pr but flow down by Gr.

References

Ahmed N., Kalita D. (2011). Transient MHD free convection from an infinite vertical plate in a rotating system with mass transfer and hall current. *Journal of Energy, Heat and Mass Transfer*, Vol. 33, pp. 271-292.

Ahmed N., Khan U., Khan S. I., Bano S., Mohyud-Din S. T. (2017). Effects on magnetic field in squeezing flow of a casson fluid between parallel plates. *Journal of King Saud University Science*, Vol. 29, pp. 119-125. https://doi.org/10.1016/j.jksus.2015.03.006

Ahmmed S. F., Biswas R., Afikuzzaman M. (2018). Unsteady magnetohydrodynamic free convection flow of nanofluid through an exponentially accelerated inclined plate embedded in a porous medium with variable thermal conductivity in the presence of radiation. *Journal of Nanofluids*, Vol. 7, pp. 891-901. https://doi.org/10.5098/hmt.11.13

Ali E. S. M. (2004). A Text book of programming in FORTRAN. Third edition. https://www.springer.com/gp/book/9783319177007

Animasaun I. L., Adebile E. A., Fagbade A. I. (2016). Casson fluid flow with variable thermo-physical property along exponentially stretching sheet with suction and exponentiallydecaying internal heat generation using the homotopy analysis method. *Journal of the Nigerian Mathematical Society*, Vol. 35, pp. 11-17. https://doi.org/10.1016/j.jnnms.2015.02.001

Attia H. A. (2005, 2006, 2007). Unsteady couette flow with heat transfer considering the ion-slip has been investigated. *European Journal of Scientific Research Recent*, Vol. 44, pp. 971-987.

Balocco C., Petrone G. (2018). Heat and moisture transfer investigation of surface building materials. *Mathematical Modelling of Engineering Problems*, Vol. 5, No. 3, pp. 146-152. https://doi.org/10.18280/mmep.050303

Biswal S., Sahoo P. K. (1994). Hall effect on oscillatory hydromantic free convective flow of a visco-elastic fluid past an infinite vertical porous flat plate with mass transfer. *Proc. Nat. Acad. Sci.*, Vol. 69A, pp. 46.

Biswas R., Afikuzzaman M., Mondal M., Ahmmed S. F. (2018). MHD free convection and heat transfer flow through a vertical porous plate in the presence of chemical reaction. *Frontiers in Heat and Mass Transfer*, Vol. 11, No. 13. https://doi.org/10.5098/hmt.11.13

Biswas R., Ahmmed S. F. (2018). Effects of Hall current and chemical reaction on MHD unsteady heat and mass transfer of Casson nanofluid flow through a vertical plate. *Journal of Heat Transfer*, Vol. 140, pp. 092402. https://doi.org/10.1115/1.4039909

Biswas R., Mondal M., Sarkar D. R., Ahmmed S. F. (2017). Effects of radiation and chemical reaction on MHD unsteady heat and mass transfer of Casson fluid flow past a vertical plate. *Journal of Advances in Mathematics and Computer Science*, Vol. 23, No. 2, pp. 1-16.

Chaware P., Sewatkar C. M. (2017). Effects of tangential and radial velocity on the heat transfer for flow through pipe with twisted tape insert-turbulent flow. *International Journal of Heat and Technology*, Vol. 35, No. 4, pp. 811-820. https://doi.org/10.18280/ijht.350417

Das S., Guchhait S. K., Jana R. N., Makinde O. D. (2016). Hall effects on an unsteady magneto-convection and radiative heat transfer past a porous plate. *Alexandria Engineering Journal*, Vol. 55, pp. 1321-1331.https://doi.org/10.1016/j.aej.2016.04.027

Garg R., Thakur H., Tripathi B. (2017). Nonlinear numerical analysis of convective-radiative fin using MLPG method. *International Journal of Heat and Technology*, Vol. 35, No. 4, pp. 721-729. https://doi.org/10.18280/ijht.350405

Hall E. (1879). On a new action of the magnet on electric currents. *American Jurnal of Mathematics*, Vol. 2, No. 3, pp. 287-292.

Hossain M. D., Samad M. A., Alam M. M. (2015). MHD free convection and mass transfer flow through a vertical oscillatory porous plate with hall, ion-slip currents and heat source in a rotating system. *Procedia Engineering*, Vol. 105, pp. 56-63. https://doi.org/10.1016/j.proeng.2015.05.006

Islam A., Biswas M. H. A., Karim M. R., Mohiuddin S. M. (2011). MHD micropolar fluid flow through a vertical porous medium. *Academic Research International*, Vol. 1, No. 3, pp. 380-393.

Kataria H. R., Patel H. R. (2016). Soret and heat generation effects on MHD casson fluid flow past an oscillating vertical plate embedded through porous medium. *Alexandria Engineering Journal*, Vol. 55, pp. 2125-2137. https://doi.org/10.1016/j.aej.2016.06.024

Kumar N. K., Masliyah J. H. (1986). Swirling flow and heat transfer in coiled and twisted pipes, Journal of American. *Advanced Transport Process*, Vol. 4, pp. 49-112. http://dx.doi.org/10.1155/2016/8235375

Makinde O. D. Khan Z. H., Ahmad R., Khan W. A. (2018). Numerical study of unsteady hydromagnetic radiating fluid flow past a slippery stretching sheet embedded in a porous medium. *Physics of Fluids*, Vol. 30, pp. 083601 (7pages). https://doi.org/10.1063/1.5046331

Makinde O. D., Khan W. A., Khan Z. H. (2017). Stagnation point flow of MHD chemically reacting nanofluid over a stretching convective surface with slip and radiative heat. *Proceedings of the Institution of Mechanical Engineers, Part E: Journal of Process Mechanical Engineering*, Vol. 231, No. 4, pp. 695-703. https://doi.org/10.1177/0954408916629506

Makinde O. D., Mabood F., Ibrahim M. S. (2018). Chemically reacting on MHD boundary layer flow of nanofluid over a non-linear stretching sheet with heat source/sink and thermal

radiation. *Thermal Science*, Vol. 22, No. 1B, pp. 495-506. https://doi.org/10.2298/TSCI151003284M

Pattnaik J. R., Dash G. C., Singh S. (2016). Diffusion- thermo effect with hall current on unsteady hydromagnetic flow past an infinite vertical porous plate. *Alexandria Engineering Journal*, Vol. 56, No. 1, pp. 13-25. https://doi.org/10.1016/j.aej.2016.08.027

Rajput K. R., Chad S. (2007). Heat and mass transfer (Multicolor edition). *S. Chad and Company Ltd*., pp. 373-387.

Rohsenow W. M., Harnett J. P., Cho Y. I. (1998). Handbook of heat transfer. 3rd edition. McGraw-Hill, New Year.

Sekhar K. R., Reddy G. V., Raju C. S. K., Ibrahim S. M., Makinde O. D. (2018). Multiple slip effects on magnetohydrodynamic boundary layer flow over a stretching sheet embedded in a porous medium with radiation and Joule heating. *Special Topics & Reviews in Porous Media: An International Journal*, Vol. 9, No. 2, pp. 117-132. https://doi.org/10.1615/SpecialTopicsRevPorousMedia.v9.i2.20

Shankar B., Yirga Y. (2013). Unsteady heat and mass transfer in MHD flow of nanofluids over stretching sheet with a nano-uniform heat source/sink. *International Scholarly and Scientific Research and Innovation*, Vol. 7, No. 12, pp. 1766-1774.

Sharma P. R. Choudhary S., Makinde O. D. (2018). MHD Slip flow and heat transfer over an exponentially stretching permeable sheet embedded in a porous medium with heat source. *Frontiers in Heat and Mass Transfer*, Vol. 9, pp. 1-7.

Sun C., Zuo Z. S., Lu W., Liu X. T., Guo X. L., Liu F. (2017). Visualization of the heat transfer character of dry slag discharge system. *International Journal of Heat and Technology*, Vol. 35, No. 4, pp. 793-798. https://doi.org/10.18280/ijht.350414

Tamoor M., Waqas M., Khan M. I., Alsaedi A., Hayat T. (2017). Magnetohydrodynamic flow of Casson fluid cylinder. *Results in Physics*, Vol. 7, pp. 498-502. https://doi.org/10.1016/j.rinp.2017.01.005

Venkateswarlu M., Makinde O. D. (2018). Unsteady MHD slip flow with radiative heat and mass transfer over an inclined plate embedded in a porous medium. *Defect and Diffusion Forum*, Vol. 384, pp. 31-48.

Wang L., Yang T. (2004). Bifurcation and stability of forced convection in curved ducts of square cross section. *Int. J. Heat Mass Transfer. European Journal of Scientific Research Recent*, Vol. 47, pp. 2971-2987. https://doi.org/10.1016/j.ijheatmasstransfer.2004.03.002

Nomenclature

x, y, z	Cartesian coordinates
u, v, w	Velocity components
U	Dimensionless primary velocity
W	Dimensionless secondary velocity
N_u	Nusselt number
α	Heat source parameter

C_f	Skin friction
ρ	Fluid density
υ	Kinematic viscosity
T_m	Mean fluid temperature,
C_s	Concentration susceptibility
S_h	Sherwood number
R_a	Radiation parameter
m	Hall parameter
$\bar{T}$	Non-dimensionlal fluid temperature
β_T	Thermal expansion coefficient
M	Magnetic parameter
P_r	Prandlt number
G_r	Grashof number
K_p	Permeability of porous medium
T	Temperature of fluid
k	Thermal conductivity
C_p	Specific heat at constant pressure